ELSEVIER

Sensors and Actuators B 38–39 (1997) 339–343

SENSORS AND ACTUATORS B CHEMICAL

Mid-infrared (3–5 μm) LEDs as sources for gas and liquid sensors

B.A. Matveev [a,*], G.A. Gavrilov [a], V.V. Evstropov [a], N.V. Zotova [a], S.A. Karandashov [a], G.Yu. Sotnikova [a], N.M. Stus' [a], G.N. Talalakin [a], J. Malinen [b]

[a] *Ioffe Physico-Technical Institute, Polytechnicheskaya 26, 194021, St. Petersburg, Russia*

[b] *VTT Electronics, Optoelectronics Laboratory, PO Box 1100, FIN-90571, Oulu, Finland*

Abstract

Mid-infrared LEDs based on InGaAs, InAsSb(P) and InGaAsSb alloys with an emission band of 0.3–0.5 μm, output power in the 10–50 μW range and long-term operation up to 20 000 h have been fabricated and tested. The LED-based analyser prototypes with PbSe photoresistors as detecting elements have been made and characterized with respect to CO, CO_2 and H_2O detection. A first attempt to make a qualitative analysis of hydrocarbons at 3.3 μm using transmission spectra recorded by an LED array spectrometer module has been undertaken.

Keywords: Infrared LEDs; Optical sensors; Spectrometers

1. Introduction

There has been an increased interest in ambient operating mid-infrared (3–5 μm) LEDs for environmental monitoring. Such sources are especially attractive for fibre-optic applications [1] and spectrometers [2–4], because of their small size and high efficiency in the spectral range where most industrial gases have fundamental absorption bands.

Previously [5] we described InGaAs- and InAsSb(P)-based LEDs for the 2.5–3.8 μm and 3.8–4.8 μm spectral regions, respectively, having emission power of 10–50 μW and FWHM of 0.3–0.5 μm and overviewed [6] most of the LEDs developed for the mid-IR region.

It was recently shown that the $In_{1-x}Ga_xAs_{1-y}Sb_y$ alloy system is a potential material for mid-IR diode lasers [6,7]. The advantages of InGaAsSb lasers are high emitting power (up to 700 mW in pulsed mode [6]) and high operating temperature [7]. However, to the best of our knowledge there are no reports on room-temperature-operating InGaAsSb LEDs emitting in the 3–5 μm spectral range.

InGaAsSb-based heterostructures have been obtained by several authors but few papers on alloys with compositions close to InAs have been published yet. The limited attention paid so far to alloy enriched with InAs can be partly explained by the weak composition dependence of the energy gap over the InAs lattice-matched line ($y=0.9x$) [8]. Therefore, a limited set of possible LED wavelengths can be obtained in conventional lattice-matched p–n structures. However, as was previously shown [9], growth of graded layers at elevated temperatures can be successfully used to manufacture alloys of high crystalline quality with a variety of energy-gap values in an InAsSb-based lattice-mismatched system.

This report presents data on A3B5 LEDs with emphasis on LEDs based on narrow-band InGaAsSb alloy grown by the LPE method at elevated temperatures. LED-based analyser prototypes designed for CO and CO_2 gases, a scale model for water detection in oil and LED array spectrometer module performance at 3.3 μm are described.

2. LED and material characterization

InGaAs, InAsSbP and $In_{1-x}Ga_xAs_{1-y}Sb_y$ ($0 \le x \le 0.15$, $0.05 \le y \le 0.135$) graded layers were grown at 650–720°C by the LPE method on n-InAs (111) substrates. Zn or Mn was used as a p-dopant for p–n junction formation during the growth.

Stress measurements performed by recording the polarization of photoluminescence emitted from the structures with a profiled substrate indicate that InGaAsSb has the highest residual stress ($\epsilon \approx 0.2\%$) compared to InAsSb and InAsSbP solid solutions, the initial stress being the same. This can be attributed to elevated hardness [10] and small plasticity of the alloy. Small InGaAsSb plasticity is also manifested in an inversed dislocation distribution over graded heterostructures grown on relatively thin (100–300 μm) substrates. The dislocation density in the graded layer of ≈30 μm thickness

* Corresponding author. Phone: +812 247 7446. Fax: +812 247 4324. E-mail: bmat@iropt3.ioffe.rssi.ru.

PII S0925-4005(97)00048-8

declines from 10^7 to 10^4 cm^{-2} with decreased substrate thickness, a fact assumed to be due to the specific feature of a graded crystal unit cell [9]. Reduction of dislocation density in epitaxial layers is accompanied by heterostructure bending and an increase of dislocation density in the InAs substrate from 10^4 to 10^7 cm^{-2}.

The photoluminescence (PL) spectral width (FWHM) and peak temperature shift (dE) both depend on the dislocation density (see Fig. 1). A possible reason why the temperature shift decreases in highly dislocated layers is tail formation in the energy gap due to disturbances caused by dislocation networks. As the temperature increases the Fermi distribution broadens, increasing the occupation probability for higher-energy states. Similar states contribute to an additional long-wave shoulder on the PL spectra of plastically deformed n-InAs substrate, which is the closest to InGaAsSb binary material. The same behaviour is typical for the temperature dependence of LED electroluminescence (EL) spectra in the 3.8–4.3 μm spectral range; for instance, the temperature drift of the EL peak is close to zero for highly dislocated epitaxial layers with $N \approx 10^7$–10^8 cm^{-2}.

The external quantum efficiency of the LEDs from InGaAsSb/InAs p–n structures appeared to be several times higher than that of homo-InAs LEDs of the same energy gap (EL peak at 3.72 μm at room temperature [11]). This is believed to be due to the disturbance of the Auger resonance non-radiative recombination in InAs-based materials [12]. LEDs fabricated from lattice-matched heterostructures ($x=y=0.07$) exhibit lowest dislocation density ($N<10^4$ cm^{-2}), maximum output power (30 μW at 100 mA) and emission peak temperature drift (3.4 nm °C^{-1}) close to the InAs energy-gap variation. Similar correlation between dislocation density and device parameters was also found for InGaAsSb-based diode lasers [13].

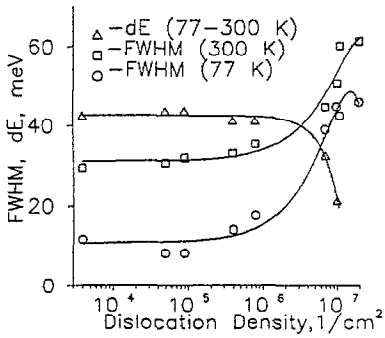

Fig. 1. Photoluminescence spectrum FWHM and temperature peak shift (77–300 K) vs. dislocation density for InGaAsSb/InAs heterostructures.

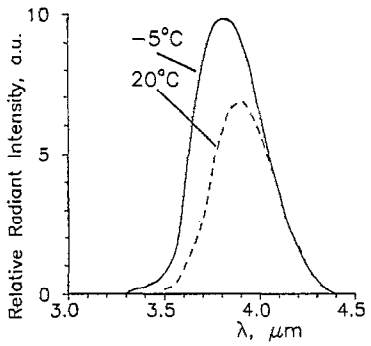

Fig. 2. Electroluminescence spectra for 3.9 μm LED at room temperature and at −5°C (thermoelecric cooling).

Fig. 2 presents the temperature variation of the emission spectrum of one of the 3.9 μm LEDs, which is typical for long-wave emitters grown on InAs substrate by LPE. Fig. 3 shows the current–voltage characteristics of our LEDs including the above 3.9 μm LED. As seen from Fig. 3, the forward current is increasing with the wavelength, manifesting the decrease of the alloy band gap.

To increase the emitted power (by a factor from three to five) LED chips were coated by As-, S- and Se-enriched glass having a refractive index ($n=2.6$) smaller than InAsSb(P) or InGaAs ($n=3.5$). Life tests involving the temperature cycling of glass-sealed InAsSb LEDs in wet air within the +10 to +40°C range indicated tolerance of these LEDs to air humidity (90%).

Most of the LED applications call for long-term operation of the latter; however, until now there are only the 100 h test results briefly mentioned in Ref. [1].

The lifetime tests (see Fig. 4) were performed on a group of $In_{0.94}Ga_{0.06}As$ LEDs (EL peak at 3.3 μm) at a pulse current of 1 A (50 μs, 30 Hz). Each 'triple' time point in Fig. 4

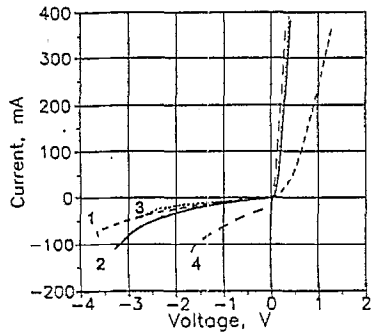

Fig. 3. Current–voltage characteristics for 3.3 (1), 3.9 (2), 4.3 (3) and 4.7 μm (4) LED at room temperature.

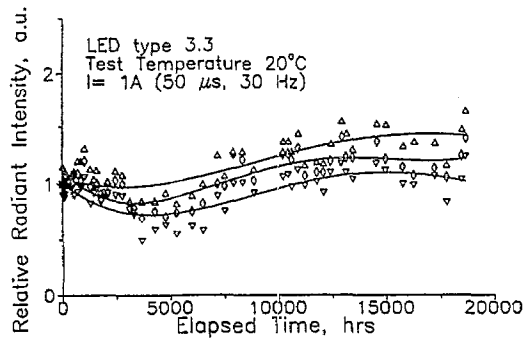

Fig. 4. Relative radiant intensity of the LEDs during long-term operation. For each lot of LEDs and for each time point three intensity data are presented: the 'best one' data, i.e., the intensity of an LED for which only 10% of all LEDs from the lot are brighter then this particular one (upper curves), the 'mean one' data representing the average LED (curves in the middle) and the 'worst one' data, reflecting an LED for which 90% of all LEDs from the lot are brighter (bottom curves).

Table 1
Gas sensor characterization

Gas	Gas absorption line max., λ_{max}, μm	Gas FWHM $\Delta\lambda_G$, μm	$\Delta\lambda_G/\Delta\lambda_{LED}$	Gas absorption coefficient, cm^{-1}		Power P_{pulse}, mW	S_λ, V W^{-1}	SNR, Ψ_{pulse}	Detection limit C_{min}, ppm	
				α_{max}	α_{eff}				single pulse	averaging time 5 s
CO_2	4.3	0.125	0.25	1.65	0.16	0.7	1400	200	7.5×10^3	5×10^2
CO	4.7	0.25	0.6	0.18	0.06	0.3	200	20	3×10^5	2×10^4

presents the intensity of the 'brightest', the 'mean' and the 'weakest' LED, respectively. These tests have indicated a slight decrease (by ≈20%) of the InGaAs LED emitting power after 5000 h of operation and a subsequent increase (by ≈30% compared to the initial value) after 15 000 h of operation. The non-monotonic behaviour of the LED efficiency may be attributed to the multiplying and further annihilation of dislocations with opposite sign.

3. Analyser prototypes

Non-dispersive IR analysers are based on a sensor head [14] that consists of sample and reference PbSe photoresistors ($R=300$ kΩ, 300 K) as detecting elements and several LED chips all mounted together on the same thermoelectric cooler (TEC) as shown in Fig. 5. The LED emission (4.3 μm for CO_2 and 4.7 μm for CO detection) was focused onto the sample photodetector by a concave mirror. The mirror was isolated from the gas by a ZnS window limiting the sample path length to 6 cm. To utilize the LED emission edge, a microreflector has been mounted together with the LEDs.

The typical analyser detection limit, that is, the smallest gas concentration C_{min} that causes a noticeable sample signal deviation (which is of the same order as the system noise) has been derived from the PbSe sensitivity (S), LED emission power (P) at $I=1$ A, FWHM and gas absorption parameters (α_{max}, FWHM) and is presented in Table 1. Estimations have been made for a single LED pulse and for an averaging time of 5 s at a pulse duration of 30 μs and 30 Hz repetition rate, which are typical operating parameters for our gas monitors. Table 1 also gives the effective absorption coefficient (α_{eff}), which takes into account overlapping of adsorption bands and LED emission spectra. Optical system efficiency at zero gas concentration was postulated to be around 0.1.

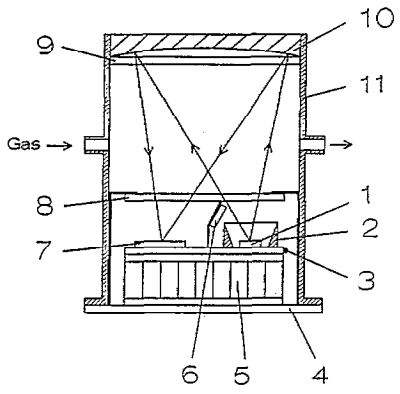

Fig. 5. IR gas-sensor configuration: 1, IR LEDs; 2, microreflector; 3, thermosensor; 4, TO-3 header; 5, TEC; 6, reference photodetector; 7, sample photodetector; 8, sapphire window; 9, protection window; 10, spherical mirror; 11, gas chamber.

As seen from Table 1, the LED emission is broader than the absorption bands for both CO_2 and CO gases ($\Delta\lambda_G/\Delta\lambda_{LED}<1$) and the intensity transmitted through the gas is, therefore, a sum of strongly absorbed wavelengths at gas absorption line maximum and neighbouring weakly absorbed wavelengths resulting in $\alpha_{eff}/\alpha_{max}<1$ and, as a consequence, in weak light-intensity variation with gas concentration.

The performance of the above-described sensor with a response time of about 5 s is demonstrated in Fig. 6 by the relative sample light intensity (monitor signal) versus gas concentration. For each gas the monitor signal is plotted as a ratio of sample and reference photocurrents at an LED/detector temperature of about $+5\pm0.1$°C. A monitor signal of unity corresponds to zero gas concentration. CO measurements have been made utilizing car exhaust and a standard IR filter analyser for gas calibration. For CO_2 tests standard samples were used.

As seen from Fig. 6, the CO_2 gas monitor is characterized by fairly good resolution at low concentrations and a wide measuring range (0.01–100%). This is a consequence of the high CO_2 absorptivity and high efficiency of both LED and detector at 4.3 μm compared to those at 4.7 μm (see Table 1).

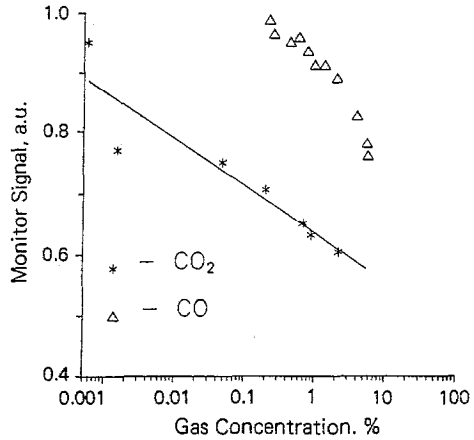

Fig. 6. Monitor responses vs. CO_2 and CO concentration. Optical path 6 cm.

When using a narrow-band filter it is possible to increase the effective absorption coefficient as described in Ref. [15]. However, this will not bring benefits in terms of resolution limits because emission narrowing through cutting off wavelengths of small absorptivity and subsequent reduction of optical power result in a signal/noise ratio decrease. Both contributions (the increase of absorption and reduction of sample beam power) are keeping the resolution limit at nearly the same level down to a filter transmission FWHM of about 0.1 μm. At FWHM < 0.1 μm a poor detection limit is expected.

For the above reasons the developed LEDs are advantageous for liquid analysis because of broad-band absorption of the liquids. For example, water can be optically detected when utilizing the strong absorption band at 2.95 μm with a FWHM of about 0.8 μm. In the water monitor prototype a differential scheme utilizing an LED with two chips mounted together on one TO-18 header emitting at 3 μm (sample beam) and 3.9 μm (reference beam), respectively, has been used. Both LED beams passed through the ≈300 μm thick liquid cell and were received by a PbSe detector. The calculated resolution was ≈0.01% H_2O, which was far below our sample concentrations (0.5% and 2% water in oil). On increasing the water content in oil from 0.5 to 2%, the sample/reference signal ratio decreased from 0.97 to 0.67, indicating the possibility of measuring the humidity of nearly 'dry' liquids ($c \ll 0.1\%$).

In many applications the presence of interfering gases calls for better spectral resolution than that simply achieved by detecting the average absorption of the sample over the whole emission band of an LED source. Previously [2] we described a seven-channel miniature grating spectrometer module designed at VTT Electronics utilizing an infrared LED array with a resolution of about 2(FWHM) ≈ 120 nm at wavelengths around 3.3 μm. Here we present preliminary data on the performance of an LED spectrometer consisting of a 15-element monolithic InGaAs LED array with element sizes of 0.45 mm × 0.45 mm and a total length of 7.5 mm emitting at 3.3 μm, a spherical concave mirror ($f = 22$ cm) and a flat grating with 200 lines/mm (see Fig. 7).

Fig. 8 presents pure methane (optical path ≈ 2 cm), acetone and ethanol (thickness ≈20–40 μm for both liquids) transmission spectra obtained through sequential activation of LED array elements and recording the transmitted radiation by a PbSe detector. The absence of fine methane absorption structure is attributed to the cross-talk of elements in the array. Nevertheless, as seen from Fig. 8, the above substances are easily distinguished from one another when using the LED array spectrometer transmission data. It is believed that by using a non-monolithic LED array [2] it would be possible to improve the device spectral resolution and performance in the promising mid-infrared analytical region.

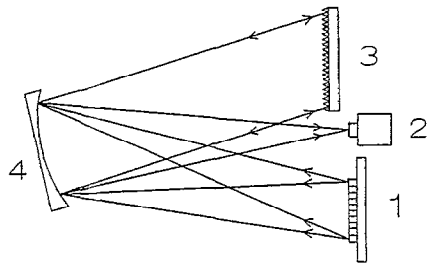

Fig. 7. Spectrometer schematic: 1, LED array; 2, photodetector; 3, flat grating; 4, spherical concave mirror.

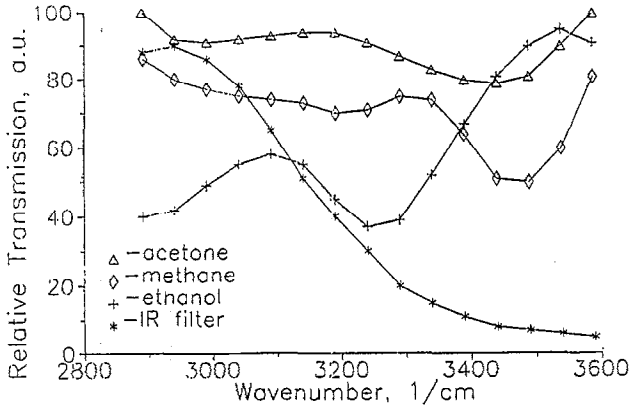

Fig. 8. Relative transmission of methane (optical path 2.5 cm), acetone and alcohol (≈0.03 mm path for both of them) recorded by 15-element LED array spectrometer. Optical filter transmission was used for spectrometer wavelength calibration.

4. Conclusions

Recently developed mid-IR LEDs based on A3B5 alloys can be currently obtained with any desired emission wavelength in the spectral range 2.5–4.8 μm. This has made it possible to replace thermal sources and rotating chopper wheels with LED sources in the design of new spectroscopic analysers with long-term operation.

Non-dispersive analysers have been developed for CO_2, CO and water detection utilizing LEDs and PbSe detectors.

An infrared spectrometer based on a linear LED array emitting at 3.3 μm and a fixed grating monochromator has been demonstrated. This construction can be used as an electrically scanned spectrometer module in future IR analysers for process on-line monitoring applications and multicomponent analysis.

Acknowledgements

The authors are grateful to M. Aidaraliev, A.V. Lunev and V.V. Shustov for technical assistance.

References

[1] S. McCabe and B.D. MacCraith, Novel mid-infrared LED as a source for optical fibre gas sensing, *Electron. Lett.*, *29* (1993) 1719–1721.

[2] J. Malinen, T. Hannula, N.V. Zotova, S.A. Karandashov, I.I. Markov, B.A. Matveev, N.M. Stus' and G.N. Talalakin, Nondispersive and multichannel analyzers based on mid-IR LEDs and arrays, *Proc. SPIE*,

Vol. 2069, *Optical Methods for Chemical Process Control*, 1993, pp. 95–101.
[3] H. Karanen and J. Malinen, *US Patent No. 5 029 245* (1991).
[4] B.A. Matveev et al., *Russian Patent No. 1 672 814* (1989).
[5] N.V. Zotova, S.A. Karandashev, B.A. Matveev, A.V. Pentsov, S.V. Slobodchikov, N.N. Smirnova, N.M. Stus', G.N. Talalakin and I.I. Markov, Optoelectronic sensors based on narrow band A3B5 alloys, *Proc. SPIE*, Vol. 1587, *Chemical, Biochemical, and Environmental Fiber Sensors III*, 1992, pp. 334–345.
[6] B.A. Matveev, M. Aidaraliev, N.V. Zotova, S.A. Karandashov, N.M. Stus' and G.N. Talalakin, Midwave (3–5 μm) III–V infrared LEDs and diode lasers as a source for gas sensors, *Proc. SPIE*, Vol. 2506, *Air Pollution and Visibility Measurements*, 1995, pp. 796–802.
[7] D.Z. Garbuzov, R.U. Martinelli, R.J. Menna, P.K. York, H. Lee, S.Y. Narayan and J.C. Connolly, 2.7-μm InGaAsSb/AlGaAsSb laser diodes with continuous-wave operation up to −39°C, *Appl. Phys. Lett.*, *67* (1995) 1346–1348.
[8] T.K. Glisson, J.R. Hauser, M.A. Littlejohn and C.K. Williams, Energy bandgap and lattice constant contours of III–V quaternary alloys, *J. Electron. Mater.*, *7* (1978) 1–16.
[9] B.A. Matveev, N.M. Stus' and G.N. Talalakin, Inverse defect formation during growth of epitaxial InAsSbP/InAs structures, *Sov. Phys. Crystallogr.*, *33* (1988) 124–127.
[10] B.A. Matveev, N.M. Stus', G.N. Talalakin, T.V. Chernin and Yu.A. Fadin, Microhardness of semiconductor alloys InGaAs, InGaAsSb and InAsSbP enriched with indium arsenide, *Inorg. Mater.*, *26* (1990) 541–543.
[11] *Infrared Light Emitting Diodes*, Laser Monitoring Systems Limited data sheet.
[12] I.V. Kryukova, V.I. Leskovich and A.V. Matveenko, Mechanism for recombination of nonequilibrium carriers in an $In_xGa_{1-x}As_ySb_{1-y}$ solid solution with electron beam pumping in the region 1.6–3 μm, *Sov. Tech. Phys. Lett.*, *5* (1979) 294–296.
[13] T.S. Argunova, R.N. Kutt, B.A. Matveev, S.S. Ruvimov, M.M. Stus' and G.N. Talalakin, Strain distribution in the binary heterostructures InAsSbP/InGaAsSb, *Phys. Sol. State*, *36* (1994) 1633–1636.
[14] B.A. Matveev et al., Analyzer for gases and liquids, *Russian Patent Appl. No. 94 010 114* (1994).
[15] S.F. Johnston, Gas monitors employing infrared LEDs, *Meas. Sci. Technol.*, *3* (1992) 191–195.

Biographies

Boris A. Matveev is a senior researcher at the A.F. Ioffe Physico-Technical Institute. He graduated from V.I. Ulyanov/Lenin/ Electrical Engineering Institute in 1977. In the same year he joined the A.F. Ioffe Physico-Technical Institute at St. Petersburg. His Ph.D. work (1987) was devoted to an investigation of deformation in semiconductor heterostructures. Now he works on mid-IR diode lasers and non-cooled LEDs for optoelectronic IR analysers.

Gennady A. Gavrilov received his Ph.D. in physics in 1967 from Ioffe Physico-Technical Institute, Russian Academy of Sciences. His current research interests include methods of optical signal detection and signal and image processing.

Valery V. Evstropov is a senior researcher at the A.F. Ioffe Physico-Technical Institute. He received his Ph.D. from the same institute in 1973. His research interests include photoelectric, electric and electroluminescent properties of III–V compound semiconductors.

Nonna V. Zotova is a senior researcher at the A.F. Ioffe Physico-Technical Institute. She received the B.A. degree in physics from the St. Petersburg State University in 1955 and a Ph.D. degree in semiconductor physics from A.F. Ioffe Physico-Technical Institute (1964). She is working on the creation and investigation of long-wavelength lasers and LEDs for optoelectronic applications and on the investigation of radiative and non-radiative recombination in heterojunctions based on narrow-gap solid solution.

Sergey A. Karandashov is a scientific researcher at the A.F. Ioffe Physico-Technical Institute. He graduated from the Electrical Engineering Institute in 1982. His research interests include the investigation of electroluminescence and optical properties of narrow-band A3B5 alloys and mid-IR LEDs and lasers.

Galina Yu. Sotnikova received her Ph.D. in physics in 1987 from the Technical University St. Petersburg. Since 1980 she has worked in the Laboratory of Holography and Optoelectronics of Ioffe Physico-Technical Institute Russian Academy of Sciences. Her scientific interests include LEDs, image sensors and their applications to optical signal processing.

Nikolai M. Stus' is a scientific researcher at the A.F. Ioffe Physico-Technical Institute. He received the B.A. degree in physics from the Dagestan State University in 1968. He is currently working on crystal growth (LPE) of narrow-band A3B5 heterostructures.

Georgyi N. Talalakin is a senior researcher at the A.F. Ioffe Physico-Technical Institute. He received the M.S. degree in 1955 from the Polytechnical Institute, Leningrad. In 1973 he received a Ph.D. (GaAs crystal growth and characterization) at the A.F. Ioffe Physico-Technical Institute. He is currently working on epitaxial growth of narrow-band A3B5 heterostructures.

Jouko Malinen received his M.Sc. and Licentiate of Technology degrees in electrical engineering from the University of Oulu, Finland, in 1979 and 1994, respectively. He joined the Technical Research Centre of Finland (VTT) in 1984 as a research scientist and since 1994 has worked with VTT Electronics as a senior research scientist in optoelectronics. He has been involved in research and development of on-line spectroscopic analysers for the pulp and paper industry as well as portable optical instrumentation for other visible and near-infrared applications. His current research interests include LED-based spectroscopic analysers.